Journal of Materials Chemistry A

ROYAL SOCIETY OF CHEMISTRY

PAPER

View Article Online
View Journal | View Issue

Cite this: J. Mater. Chem. A, 2025, 13, 4587

Alginate–oligothiophene aerogels as photocatalysts for the degradation of emerging organic contaminants in water†‡

Andrea Trifoglio,§[ac] Francesca Tunioli,§[ac] Laura Favaretto,[a] Massimo Zambianchi,[a] Cristian Bettini,[a] Ilse Manet,[a] Livia Mariani,[b] Anna Barra Caracciolo,[b] Paola Grenni,[b] Manuele Di Sante,[cd] Matteo Di Giosia,[cd] Tainah Dorina Marforio,[cd] Edoardo Jun Mattioli,[cd] Matteo Calvaresi *[cd] and Manuela Melucci *[a]

V-shaped oligothiophenes bearing a benzothiophene (BT) core and *S*-oxide or *S*,*S*-dioxide moieties are herein proposed as photocatalysts for the degradation of three selected water emerging contaminants. Photocatalyst molecules were designed in order to minimize aggregation in the solid state (V-shape structure), lower the HOMO–LUMO gap (*S*,*S*-dioxide moiety functionalization) with respect to conventional oligothiophenes and enhance the photocatalytic performance. The targeted BT molecules were synthesized by the Stille cross-coupling reaction and their ability to generate reactive oxygen species (ROS) upon blue-light irradiation was demonstrated. For practical exploitation, BTs were embedded into an alginate matrix by ionotropic gelation–freeze drying processes to obtain porous aerogels that were dispersed in water and used for the degradation of emerging contaminants. Degradation performance of up to 99% after 2 h on ofloxacin (antibiotic), rhodamine B (dye) and bisphenol A (plastic additive), was observed. In addition, regenerated photocatalysts showed unchanged performance after five reuse cycles. The relationship between the BT molecular structure and ROS production, investigated by QM calculations, highlighted the role of the *S*,*S*-dioxide moiety in ROS generation, with ofloxacin antibiotic degradation performance reaching up to 99% for **BTO$_2$-T2**. Remarkably, ecotoxicity studies showed no toxicity of the photodegradation products toward the *Aliivibrio fischeri* bioluminescent bacterium, highlighting the potential of BT molecules for water purification.

Received 19th September 2024
Accepted 1st January 2025

DOI: 10.1039/d4ta06689h

rsc.li/materials-a

Introduction

The removal of emerging contaminants (ECs), such as per- and polyfluoroalkyl substances, pesticides, pharmaceuticals, and endocrine disruptors, has emerged as one of the foremost drinking water issues in the past decade.[1–3] The allowed limits for some of these contaminants in drinking water are continuously updated to ever-decreasing values,[4,5] posing increasingly hard challenges for the development of new remediation technologies since conventional drinking water treatment plants are not designed to remove all ECs.[6,7] Conventional treatments for the removal of emerging contaminants are mainly based on membrane technologies (nanofiltration and reverse osmosis),[8,9] advanced oxidative processes (AOPs)[10] and adsorption.[11–13] Adsorption is particularly advantageous in terms of cost and ease of use but it produces wastes to be regenerated or disposed of.[14] Despite its widespread use for desalination or point-of-use drinking water treatment, reverse osmosis still has high water rejection rates and high energy consumption.[15] AOPs include methods for the generation of hydroxyl radicals, superoxide and other reactive oxygen species (ROS), which are powerful oxidizing agents that react with harmful organic compounds, resulting into contaminant degradation. One of the most widely investigated AOPs is photodegradation, which involves the use of photocatalysts such as TiO_2, CdS and ZnO nanoparticles, *i.e.*, materials that absorb

[a]*Institute for Organic Synthesis and Photoreactivity (ISOF), National Research Council of Italy (CNR), Via P. Gobetti 101, 40129 Bologna, Italy. E-mail: manuela.melucci@isof.cnr.it; matteo.calvaresi3@unibo.it*

[b]*Water Research Institute (IRSA), National Research Council (CNR), Via Salaria Km 29, 300 C. P. 10 – 00015 Monterotondo Stazione, Rome, Italy*

[c]*Department of Chemistry 'G. Ciamician', Alma Mater Studiorum – University of Bologna, Via Selmi 2, 40126 Bologna, Italy*

[d]*IRCCS Azienda Ospedaliero – Universitaria di Bologna, Preclinical & Translational Research in Oncology Lab (PRO), Bologna, Italy*

† In memory of Giovanna Barbarella.

‡ Electronic supplementary information (ESI) available. See DOI: https://doi.org/10.1039/d4ta06689h

§ These authors contributed equally.

light and subsequently generate reactive species destroying contaminants.[16–18]

Due to their high redox potential, reactivity, efficiency, chemical stability, non-toxicity, and low cost, TiO_2-based photocatalysts are the most studied and widely employed.[19] The non-specific nature of the reactive species created upon irradiation makes TiO_2-based photocatalysts capable of degrading different classes of organic contaminants.[20–22] On the other hand, the recombination of photo-generated charge carriers, inefficient visible light exploitation, and low adsorption capacity require further optimization to boost photocatalytic potential and enable practical exploitation.[23]

In recent years, other nanomaterials, such as metal–organic frameworks (MOFs),[24] covalent organic frameworks (COFs)[25] and graphene nanosheets[26] have been proposed as photocatalysts with excellent performance due to their tuneable-by-design functionalities, high surface area and the large number of active sites available for EC degradation.[27,28] In particular, MOFs have shown remarkable performance in the degradation of organic dyes such as methylene blue and rhodamine B, *e.g.*, Fe-MOFs are able to degrade them by 100% and 94%, respectively, in 60 minutes under visible light irradiation.[29] Zr-based MOFs have also been used to degrade pesticides such as glyphosate, achieving selective degradation of 64% into sarcosine and orthophosphates.[30] MOF-C_3N_4 binary composites have been employed in the degradation of pharmaceuticals such as ofloxacin, demonstrating 96% degradation in 200 minutes.[31]

Small π-conjugated organic molecules such as porphyrin have also been used as hybrid metal–organic photocatalysts for light-assisted degradation of various organic contaminants in water.[32] Overall, porphyrins immobilized in inorganic semiconductors,[33] zeolites,[34] graphene,[35] or porous organic polymers,[36] usually exhibit improved physicochemical properties and stability, and they are active in the photodegradation of pesticides, dyes, and pharmaceuticals.[37,38] For example, Sun *et al.* reported the complete degradation of rhodamine B in just 36 minutes with the use of CuPp–TiO_2 (CuPp: mono-[4-(2-ethyl-*p*-hydroxybenzoate)ethoxyl]-10,15,20-tri(phenyl)porphyrin copper(II)).[39] The photocatalytic activity of the graphene–TiO_2–tetrakis(4-carboxyphenyl)porphyrin (3.0%) nanocomposite was tested on bisphenol A, and a degradation of 85% was observed after 240 minutes of irradiation.[40]

Here, for the first time, we propose and investigate oligothiophenes entrapped in an alginate matrix, as organic photocatalysts for the degradation of rhodamine B dye (RhB), bisphenol A (BPA) and ofloxacin antibiotic (OFLOX), three contaminants of high environmental relevance in drinking water.[41,42] RhB is a common water-soluble organic dye employed in the textile industry and its presence in water bodies has been found with concentrations ranging from ng L^{-1} to μg L^{-1}.[42] Even at very low concentrations (1.0 mg L^{-1}), it imparts a vivid colour to water, but the limit concentration to protect against hazardous effects is 140 μg L^{-1}.[43,44] BPA is a plastic additive used primarily in the production of polycarbonate plastics and epoxy resins. It is classified as an endocrine-disrupting chemical and recent research has revealed the widespread presence of BPA in groundwater, categorizing it as a ubiquitous pollutant.[45,46] OFLOX is a fluorinated quinolone antibiotic used for human and animal bacterial infections, and it has raised increasing concern due to its widespread use. OFLOX was found in surface water up to 160 μg L^{-1} and its presence in aquatic environments is associated with the potential to induce antibiotic resistance.[47]

Branched oligothiophenes (V-shaped) based on the benzo[*b*]thiophene core (BT) were introduced by G. Barbarella *et al.* as active layers for organic light emitting diodes.[48] The V-shape minimizes aggregation and related fluorescent quenching in the solid state and promotes efficient solid state photoluminescence.[48] In addition, the insertion of *S*-oxide or *S*,*S*-dioxide moieties into the aromatic backbone decreases the HOMO–LUMO energy gap.[49,50] The capability of oligothiophene molecules to produce reactive oxygen species under light stimulus has been recently exploited for cancer therapy applications.[51,52]

Here, aiming at EC degradation in water, we studied how the energy gap of the targeted BT materials family affects the generation of radicals. We synthesized a rational class of molecules having the same molecular V-shape and respectively no oxide (**BT-T2**), *S*-oxide (**BTO-T2**) and *S*,*S*-dioxide (**BTO_2-T2**) moieties (Scheme 1). **T2(BTO_2)$_3$** was synthesized with the aim of extending the π system and increasing the number of *S*,*S*-dioxide moieties to promote the generation of radicals. Finally, **BTO_2-Tz2** was synthesized by introducing electron-deficient nitrogen into the system and thus creating a push–pull system, which leads to the lowering of the HOMO–LUMO energy gap.[53]

The optical properties of BTs were investigated by spectroscopy and DFT calculations. The ROS produced upon irradiation were quantified and their generation mechanism was studied. For the technological exploitation of these insoluble compounds in water, the BT molecules were encapsulated in alginate, a safe and water processable matrix,[54,55] and used to determine the degradation mechanism toward RhB, BPA and OFLOX as well as their reusability.

Finally, to ensure water safety, we investigated the possible ecotoxicity of the photodegradation by-products of OFLOX in the presence of photocatalysts. This was performed using an

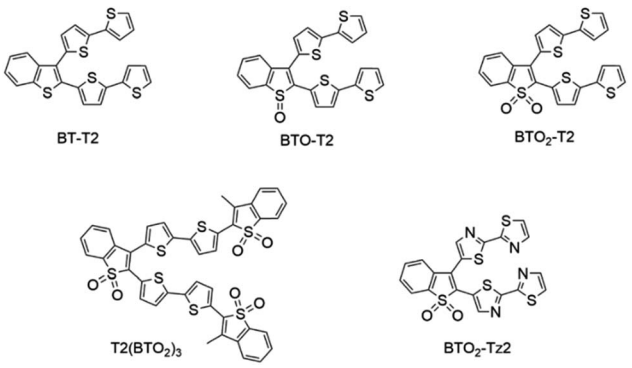

Scheme 1 Branched V-shaped (**BT-T2**) and *S*-oxide (**BTO-T2**) or *S*,*S*-dioxide (**BTO_2-T2**, **T2(BTO_2)$_3$**, and **BTO_2-Tz2**) molecules engineered for photocatalysis studies.

aquatic organism, the bacterium *Aliivibrio fischeri*, to perform an eco-toxicological bioassay.[56–58] *A. fischeri* (formerly classified as *Vibrio fischeri*) is a biosensor[59] extremely sensitive to different environmental contaminants[60,61] and it is currently used to assess water quality with standardized procedures and ecotoxicological evaluation.[62]

Experimental section

Synthesis of BT molecules

2,3-Dibromo-benzo[*b*]thiophene, 2-bromothiazole, 3-methylbenzothiophene, *n*-butyllithium (*n*-BuLi), trimethyltin chloride (Me_3SnCl), tributyltin chloride (Bu_3SnCl), *N*-bromosuccinimide (NBS), *m*-chloroperbenzoic acid (mCPBA), boron trifluoride diethyl etherate ($BF_3 \cdot Et_2O$), tetrabutylammonium bromide (TBAB), *N*,*N*-diisopropylethylamine (i-Pr_2NEt), tris(dibenzylideneacetone)dipalladium(0)-chloroform adduct ($Pd_2(dba)_3 \cdot CHCl_3$), triphenylarsine ($AsPh_3$), palladium(II) acetate ($[Pd(OAc)_2]_3$) were purchased in the highest grade available from Sigma-Aldrich Co, Milan, Italy, and were used without further purification. OFLOX (>99%), RhB (>95%) and BPA (>95%) were purchased from Sigma-Aldrich Co, Milan, Italy, and used as received.

The syntheses of 5-tributylstannyl-2,2′-bithiophene (**3**),[49] 2,3-di([2,2′-bithiophen]-5-yl)benzo[*b*]thiophene (**BT-T2**), 2,3-dibromobenzo[*b*]thiophene-1,1-dioxide (**5**), 2,3-di([2,2′-bithiophen]-5-yl)benzo[*b*]thiophene-1,1-dioxide (**BTO_2-T2**),[48] and 2,2-bithiazole[63,64] (**6**) have already been reported.

Unless otherwise noted, all operations were carried out under a dry, oxygen-free nitrogen atmosphere. Organic solvents were dried following standard procedures. Analytical thin-layer chromatography was carried out using a 0.2 mm sheet of silica 60 F_{254} (Merck, Milan, Italy). Visualization was accomplished using UV light. Preparative column chromatography was performed on glass columns of different sizes hand-packed with silica gel 60 (particle sizes 0.040–0.063 mm, Merck). We referred to ethyl acetate as EA, petroleum ether as PE, and tetrahydrofuran as THF.

The syntheses of 2,3-dibromobenzo[*b*]thiophene-1-oxide (**2**), 5-(trimethylstannyl)-2,2′-bithiazole (**6**), 2-bromo-3-methylbenzo[*b*]thiophene(**11**), 2-bromo-3-methylbenzo[*b*]thiophene-1,1-dioxide (**12**), 2-([2,2′-bithiophen]-5-yl)-3-methylbenzo[*b*]thiophene-1,1-dioxide (**13**), 2-(5′-bromo-[2,2′-bithiophen]-5-yl)-3-methylbenzo[*b*]thiophene 1,1-dioxide (**14**), and 3-methyl-2-(5′-(tributylstannyl)-[2,2′-bithiophen]-5-yl)benzo[*b*]thiophene-1,1-dioxide (**8**) are reported in Section 1.1, ESI.‡

2,3-Di([2,2′-bithiophen]-5-yl)benzo[*b*]thiophene-1-oxide (4, BTO-T2). The catalyst $Pd(AsPh_3)_4$ was generated *in situ*: a solution of $Pd_2(dba)_3 \cdot CHCl_3$ (0.01 mmol, 10.4 mg) and $AsPh_3$ (0.08 mmol, 24.5 mg) in 8 mL of toluene under a nitrogen stream was warmed to reflux, and then 0.077 g (0.25 mmol) of compound **2** (ref. 49) in 5 mL of toluene was added to the mixture. Afterwards, 0.26 g (2.3 eq., 0.58 mmol) of 5-tributylstannyl-2,2′-bithiophene **3** in 4 mL of toluene was added dropwise and the mixture was stirred for 5 h. The solvent was evaporated and the crude product was purified *via* column chromatography (silica gel, PE/CH_2Cl_2/EA 70 : 15 : 15 v/v). The isolated product was recrystallized from toluene and pentane to obtain an orange powder (0.1 g, 83% yield); mp 129 °C; DEP-EI-MS *m*/*z* 479 [$M^{\bullet+}$]; $\lambda_{max} = 430$ nm in CH_2Cl_2; $\lambda_{PL} = 571$ nm in CH_2Cl_2. ^{1}H NMR ($CDCl_3$, TMS/ppm) δ 7.96 (d, $J = 7.6$ Hz, 1H), 7.59 (d, $J = 3.6$ Hz, 1H), 7.50 (m, 2H), 7.42 (d, $J = 7.6$ Hz, 1H), 7.30 (d, $J = 3.6$ Hz, 1H), 7.29 (dd, $J = 4.0$, 1.2 Hz, 1H), 7.26 (m, 1H), 7.23 (dd, $J = 5.2$, 1.2 Hz, 1H), 7.16 (d, $J = 3.6$ Hz, 1H), 7.13 (m, 2H), 7.06 (dd, $J = 5.2$, 3.6 Hz, 1H), 6.98 (dd, $J = 5.2$, 3.6 Hz, 1H); ^{13}C NMR ($CDCl_3$, TMS/ppm) δ 143.8, 142.2, 141.1, 140.9, 140.1, 136.5, 136.4, 132.6, 131.6, 131.0, 130.6, 130.4, 130.2, 128.6, 128.0, 127.9, 126.4, 125.5, 125.3, 124.8, 124.6, 124.3, 124.0, 123.9. Anal. calcd for $C_{24}H_{14}OS_5$ (478.68): C, 60.22; H, 2.95. Found: C, 60.64; H, 2.81.

2,3-Di([2,2′-bithiazol]-5-yl)benzo[*b*]thiophene-1,1-dioxide (7, BTO_2-Tz2). The catalyst $Pd(AsPh_3)_4$ was generated *in situ*: a solution of $Pd_2(dba)_3 \cdot CHCl_3$ (0.04 mmol, 41.4 mg) and $AsPh_3$ (0.32 mmol, 97.9 mg) in 40 mL of toluene under a nitrogen stream was warmed to reflux, and then 0.324 g (1.0 mmol) of compound **5** in 10 mL of toluene was added to the mixture. Afterwards, 0.96 g (85 wt%, 2.15 eq., 2.15 mmol) of compound **6** in 5 mL of toluene was added dropwise and the mixture was stirred for 5 h. The solvent was evaporated and the crude product was purified by column chromatography (silica gel, PE with increasing amounts of EA, from 60 : 40 to 0 : 100 v/v). The isolated product was recrystallized from toluene and pentane to obtain a yellow powder (0.33 g, 67% yield); mp 140 °C; DEP-EI-MS *m*/*z* 498 [$M^{\bullet+}$]; $\lambda_{max} = 403$ nm in CH_2Cl_2; $\lambda_{PL} = 530$ nm in CH_2Cl_2. ^{1}H NMR ($CDCl_3$, TMS/ppm) δ 8.52 (s, 1H), 8.02 (s, 1H), 7.97 (d, $J = 3.2$ Hz, 1H), 7.91 (m, 1H), 7.87 (d, $J = 3.2$ Hz, 1H), 7.64 (m, 2H), 7.57 (d, $J = 3.2$ Hz, 1H), 7.49 (d, $J = 3.2$, 1H), 7.41 (m, 1H); ^{13}C NMR ($CDCl_3$, TMS/ppm) δ 165.3, 163.9, 160.6, 160.4, 146.2, 145.5, 144.4, 144.4, 135.4, 134.4, 133.8, 132.6, 130.9, 127.3, 126.2, 124.9, 124.0, 122.4, 122.3, 122.0. Anal. calcd for $C_{20}H_{10}N_4O_2S_5$ (498.63): C, 48.18; H, 2.02. Found: C, 48.41; H, 2.19.

2,2′-((1,1-Dioxidobenzo[*b*]thiophene-2,3-diyl)bis([2,2′-bithiophene]-5′,5-diyl))bis(3-methyl benzo[*b*]thiophene-1,1-dioxide) (9, T2(BTO_2)$_3$). The catalyst $Pd(AsPh_3)_4$ was generated *in situ*: a solution of $Pd_2(dba)_3 \cdot CHCl_3$ (0.008 mmol, 8.3 mg) and $AsPh_3$ (0.064 mmol, 19.6 mg) in 8 mL of toluene under a nitrogen stream was warmed to reflux, and then 0.065 g (0.20 mmol) of compound **5** in 4 mL of toluene was added to the mixture. Afterwards, 0.29 g (2.3 eq., 0.46 mmol) of compound **8** in 2.5 mL of toluene was added dropwise very slowly and the mixture was stirred for 5 h. The reaction crude was centrifuged, the supernatant was removed, and the precipitate was washed with pentane (2 × 10 mL). The purification process involved many washing/centrifugation steps during which the solid was treated sequentially with boiling CH_2Cl_2, boiling toluene, boiling dioxane, and methanol. After a final wash with pentane a poorly soluble orange powder was isolated in 76% yield (0.13 g): mp > 300 °C; DEP-EI-MS *m*/*z* 850 [$M^{\bullet+}$]; $\lambda_{max} = 452$ nm in CH_2Cl_2; $\lambda_{PL} = 541$ nm in CH_2Cl_2. ^{1}H NMR (DMSO-d_6, TMS/ppm, 40 °C) δ 8.10 (m, 1H), 7.94 (m, 2H), 7.84–7.73 (m, 7H), 7.68–7.58 (m, 8H), 7.55 (d, $J = 4.0$ Hz, 1H), 7.53 (d, $J = 4.0$ Hz, 1H), 2.52 (s, 3H), 2.48 (s, 3H). Anal. calcd for $C_{20}H_{10}N_4O_2S_5$ (498.63): C, 48.18; H, 2.02. Found: C, 48.41; H, 2.19.

Preparation of alginate–BT aerogels

BTs were embedded in an alginate (ALG) matrix by ionotropic gelation technique, according to a previously reported method.[65] Sodium alginate (50 mg, 1% w/v) and the desired BT (10 mg, 0.2% w/w) were dispersed in 5 mL of ultrapure water and sonicated for 2 h. The suspension was extruded as small drops using a Gilson pipette (1000 μL) into a gently stirred aqueous solution of calcium chloride ($CaCl_2$, 0.2 M). The distance between the pipette tip and the collection bath was approximately 30 mm. To minimize aggregation the obtained hydrogel beads were kept at room temperature under gentle agitation for 12 h. After removing water by filtration, the beads were washed three times with mQ water, and then subjected to freeze-drying to obtain aerogel beads. The total water content of the beads was determined gravimetrically by measuring the difference in weight before and after drying a portion of the beads in an oven at 100 °C until a constant weight was reached and the water content was found to be approximately 93%. The wet beads produced in this study had a size of 3–4 mm, while the final freeze-dried beads had a diameter ranging from 1.5 to 2.5 mm. The BT loading was quantitative, *i.e.*, no trace of BT was found in the water–$CaCl_2$ solution, meaning that the average concentration of BT in the beads was 16.7% (w/w) BT : alginate. In a typical experiment, about 200 beads with 3.5 mm (±0.5 mm) diameter were obtained, meaning that the BT content in a single bead was approximately 50 μg (with an Alg content of 250 μg).

Theoretical calculations

All computations were carried out using the Gaussian16 series of programs.[65] The geometry of the oligothiophene molecules was optimized in DMSO using the IEF-PCM solvation model,[66] using the DFT Minnesota functional M06-2X in conjunction with the 6-31+G* basis set (M06-2X/6-31+G*). The first excited state (S_1) was calculated considering a vertical transition from the optimized ground state (S_0) structure, using time-dependent DFT formalism (TD-DFT) with the long-range corrected hybrid functional CAM-B3LYP[67] and the 6-31+G* basis set (TD-CAM-B3LYP/6-31+G*). This combination effectively reproduces the photophysical properties of oligothiophene molecules.[52,68]

Optical properties and confocal microscopy

Absorption spectra were recorded on a spectrophotometer PerkinElmer λ_{950} with a 1 cm quartz cuvette. Reflectance spectra of the beads were recorded on the same spectrophotometer with and integrating sphere and a 1 cm quartz cuvette. Fluorescence spectra were measured on an Edinburgh Spectrofluorimeter FLSP920 with 2 nm steps and 0.5 s dwell time. The slits were set to 2–3 nm for both excitation and emission. Right angle detection was used. All the measurements were carried out at 295 K in quartz cuvettes with a path length of 1 cm. All fluorescence spectra were obtained for air-equilibrated solutions with absorbance less than 0.1 and corrected for the wavelength dependent response of the monochromator/PMT couple. Fluorescence lifetimes were measured in air-equilibrated solutions with a time correlated single photon counting system. A pulsed Hamamatsu 405 nm laser source with a 1 MHz repetition rate was used for excitation and the emission was collected at a right angle at 520 nm (**BT-T2**, **BTO_2-Tz2**), and 620 nm for the others. Decay profiles were fitted using a multiexponential function with deconvolution of the instrumental response.

Fluorescence confocal imaging was performed on an inverted Nikon Ti-E microscope (Nikon Co., Shinjuku, Japan). The confocal fluorescence microscope Nikon A1 is equipped with an argon ion CW laser as well as 405 nm and 485 nm pulsed diode lasers (PicoQuant GmbH, Berlin, Germany). Images were collected using a Nikon Plan Apo VC 60× objective with NA 0.9. Filters were set to register fluorescence in the 500–540, 560–630 nm and 660–740 nm ranges. Fluorescence imaging was completed with differential interference contrast (DIC) images.

Spectral imaging was performed with the Nikon spectral mode with a 32-PMT array detector. Wavelengtth resolution was set to 10 nm per PMT and the membranes were excited either at 488 nm or 405 nm.

Fluorescence lifetime imaging was performed by exciting with a pulsed 405 or 485 nm diode laser and collecting photons with an integrated PicoHarp 300 electronic system (PicoQuant GmbH, Berlin, Germany) for TCSPC measurements. A single-photon avalanche diode detector equipped with a bandpass filter was used as the detector. Histograms of the collected photons consist of 3200 channels, each with 16 ps width. The repetition rate of the pulsed excitation was 20 MHz. The instrument response function of the system is approximately 220 ps. The fluorescence decay fit was performed on the histogram calculated for a region of interest. The fluorescence decay profile was analyzed with a least-squares method, using a biexponential decay function provided by Picoquant SymPhoTime software.

The fitting function used is

$$I(t) = b + \sum_j a_j \exp(-t/\tau_i) \quad (1)$$

The fractional intensity and the average fluorescence lifetime are calculated according to the following equations:

$$f_i = a_i\tau_i \Big/ \sum_j a_j\tau_j \quad (2)$$

$$\tau_{av} = \sum_j f_j\tau_j \quad (3)$$

Photodegradation experiments

All the photodegradation experiments were performed using a blue LED stripe (λ_{EM} = 461 nm, irradiation power density = 10 mW cm^{-2}, and a distance of about 10 cm) and the set-up is depicted in Fig. 6. 5 mg of photocatalysts (aerogels containing BTs) were added to 3 mL of a solution of RhB, BPA or OFLOX (4 mg L^{-1} in ultrapure water). Samples were stirred under blue light irradiation for 5 h; during this time 200 μL aliquots were collected every hour and each sample was analysed by HPLC. Reuse tests were performed on Alg–**BTO_2-T2**, Alg–**BTO_2-Tz2** and

Alg–**T2(BTO$_2$)$_3$** aerogels. After the first photodegradation experiment, the aerogels were externally dried on filter paper, washed with deionized H_2O, and reused in a new photodegradation test (3 mL of a spiked solution at 4 mg L^{-1}). The procedure was repeated for a total of five cycles.

Results and discussion

Synthesis of BT molecules and alginate aerogel preparation

The synthesis of BT molecules was carried out *via* Stille coupling between dibromo derivatives **2** and **5** and the appropriate stannane (Scheme 2a). The reactions were carried out in refluxing toluene using *in situ* prepared Pd(AsPh$_3$)$_4$ as the catalyst.[48] Compounds **2** and **5** were synthesized starting from commercially available 2,3-dibromo-benzo[*b*]thiophene (**1**) by reaction with mCPBA and $BF_3 \cdot Et_2O$ (yielding 76% and 90% for 2 and 5, respectively). Compound **4** was synthesized by Stille coupling between dibromo derivative **2** and stannane **3**, yielding 83%. Stannyl-derivative **8** was synthesised starting from methyl benzothiophene **10** through a five step procedure. Compound **10** was first reacted with NBS in AcOH/CH_2Cl_2 to give the brominated adduct **11**. Oxidation of by mCPBA in

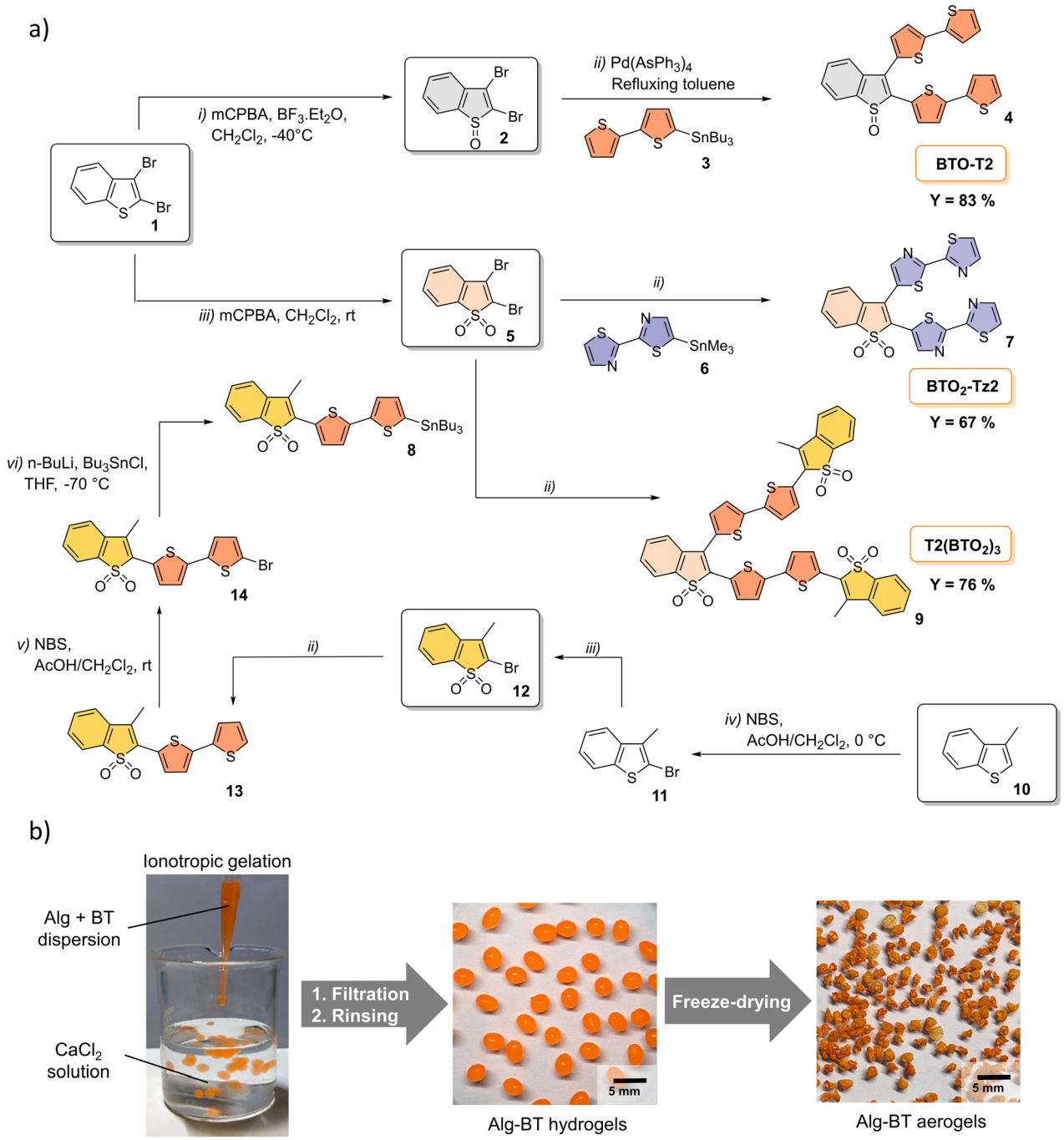

Scheme 2 (a) Synthesis of V-shaped BT oligomers. (b) Preparation of BTs–alginate aerogels by the ionotropic gelation method.

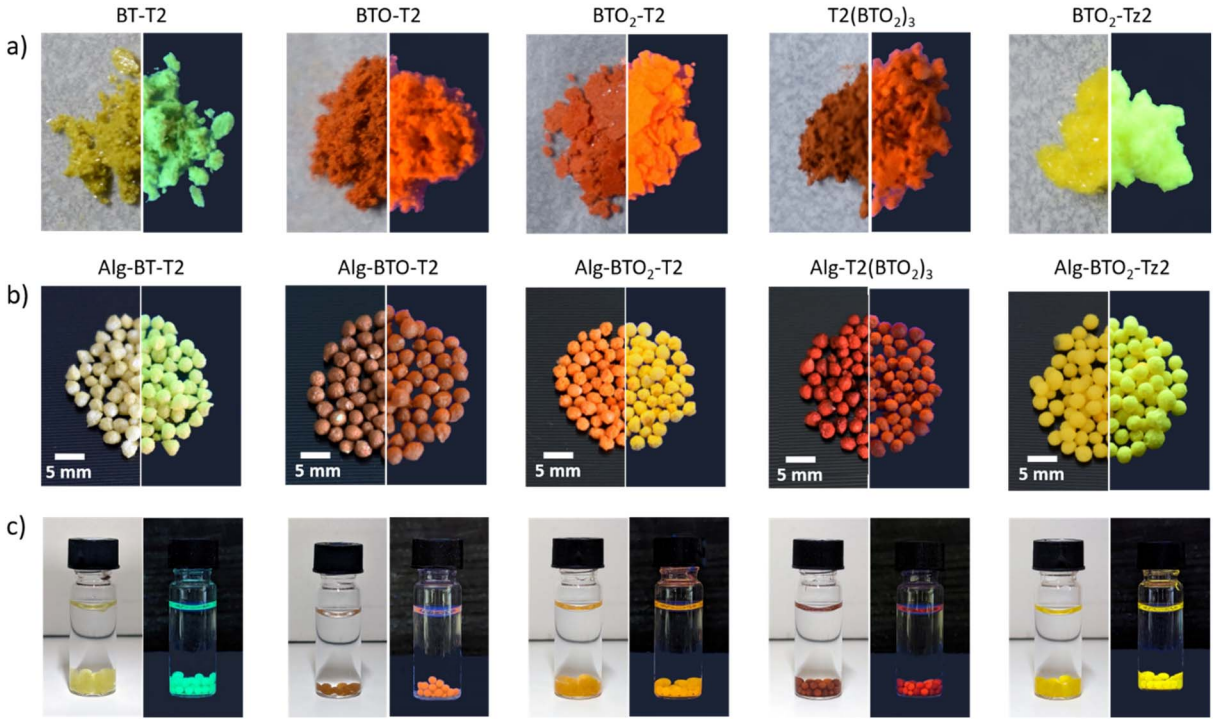

Fig. 1 Images of BT powders (top), alginate aerogels (middle) and dispersion (bottom, after 5 days from preparation) in water under white light (left) and under UV light with emission at 365 nm (right).

dichloromethane afforded the targeted sulphone derivative **12** in excellent yields (90%). The Stille coupling reaction of compound **12** with distannyl bithiophene **3** afforded **13** in 91% isolated yield. After bromination of compound **13** and subsequent stannylation, Stille coupling with dibromo-benzothiophene-*S*,*S*-dioxide **5** afforded V-shaped BT oligomers **7** and **9** in 67% and 76% yields, respectively. **BT-T2** and **BTO_2-T2** were synthesized under already described conditions and obtained in 48% (**BT-T2**) and 90% (**BTO_2-T2**).[48]

Due to the poor solubility of oligothiophenes in water, BT molecules were embedded in an alginate matrix[54,69] by the ionotropic gelation method (Scheme 2b). In detail, sodium alginate and BT molecules in powder form (ratio 5 : 1 w/w) were dispersed in water and sonicated for 2 h to obtain a homogeneous suspension which was added dropwise into a $CaCl_2$ solution. Finally, hydrogels were freeze-dried to produce the corresponding aerogels (Alg–BT, Fig. 1). All experimental details on characterization are reported in Section 1.2, ESI.‡

Fig. 1 shows images of BT powders, Alg-beads and their dispersion under normal and UV light. The different powders are mostly yellow, orange and red in colour and show strong emission when exposed to UV irradiation. The reflectance spectra shown in Fig. S1, ESI‡ are in line with the bead colors.

Furthermore, Fig. 1 (bottom line) shows that when Alg–BT aerogels are dispersed in water, there is no leaching from the alginate matrix even after 5 days of contact time, making them suitable candidates for water treatment purposes since they can be dispersed but not dissolved in water. The morphology of the Alg–BT aerogels was studied by scanning electron microscopy (SEM), as shown in Fig. 2. All the samples showed the typical micrometric porous structure of alginate aerogel with a dense skin layer.

Fig. 2b shows the cross-section of the pristine alginate bead and Alg–**BTO_2-T2** bead, taken as a case study, demonstrating that the porous structure of pristine alginate is maintained after the ionotropic gelation and freeze-drying processes. The porous structure of Alg–BT can favour the penetration of contaminant molecules into the bead and the concomitant interaction with the photocatalysts. Noteworthily, the ability of alginate hydrogels to adsorb contaminants has already been demonstrated by some of us for alginate–graphene composites and for amino-modified alginate hydrogels.[55,70] The morphology was further explored by means of confocal fluorescence and spectral

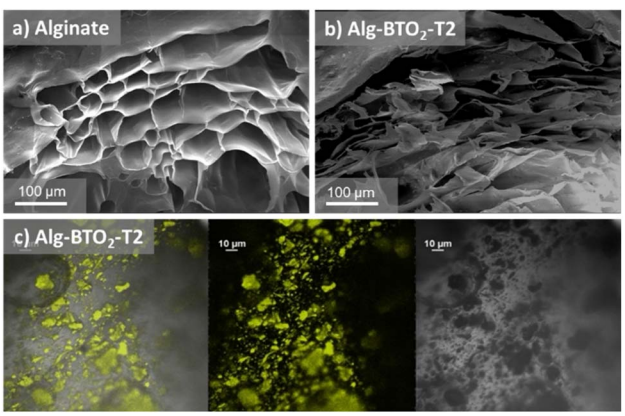

Fig. 2 SEM images of (a) pristine alginate aerogel, and (b) alginate–BTO_2-T2 aerogel. (c) Confocal fluorescence image and differential interference contrast microscopy (DIC) image of BTO_2-T2 beads.

imaging. All beads exhibit emission from the loaded oligothiophene. The images of all beads (Fig. 2c and S2‡) show that BT molecules tend to accumulate in aggregates of μm size on the beads.

Optical properties and confocal microscopy

The optical properties of BT molecules were investigated by UV-vis and fluorescence spectroscopy in CH_2Cl_2 and PBS with 5% DMSO (Fig. S3, ESI‡). Fig. 3a gives an overview of the optical behaviour of the studied BT molecules in CH_2Cl_2 solution highlighting the typical fluorescence under blue light irradiation. The absorption spectra of the BT molecules in CH_2Cl_2 and PBS/DMSO are shown in Fig. 3b and S3a.‡ All BT molecules absorb in the violet–blue range of the visible spectrum and exhibit two distinct peaks corresponding to electronic transitions from the ground state to the first and second excited state. The insertion of *S*-oxide or *S*,*S*-dioxide moieties results in a red-shift of the absorption wavelength, as shown by the λ_{abs} of **BT-T2** (375 nm), **BTO-T2** (430 nm) and **BTO_2-T2** (430 nm). The extension of the conjugated π-system and the presence of two other *S*,*S*-dioxide moieties in **T2(BTO_2)$_3$** lead to a further red-shift (λ_{abs} = 460 nm). The introduction of a push–pull system in **BTO_2-Tz2**, compared to **BTO_2-T2**, leads to a blue-shift (403 nm *vs.* 430 nm).

The spectra calculated at the TD-CAM-B3LYP/6-31+G* level (see computational details) well reproduce the experimental ones (Fig. S4 and Table S2‡), validating the accuracy of the calculations. DFT optimization of the molecules indicates that in the most stable conformation, the BT ring and the thiophene at BT position 2 are conjugated and remain planar while the thiophene substituent at BT position 3 adopts an orthogonal orientation (Fig. 3c). This structural characteristic affects the nature of the $S_0 \rightarrow S_1$ transitions of the different molecules, because they are localized only on the planar core of the molecules, where the π-conjugation is maximized (π–π* transitions). The molecular orbitals (MOs) involved in the electronic transition were calculated (Fig. S5‡). The transitions with the larger oscillator strength (Table S2‡) correspond to the experimental bands with higher molar extinction coefficients. Jablonski diagrams of the thiophene derivatives (Fig. 4) showed that the calculated T_1 excited states (Table 1) are at higher energies than the singlet excited state of the oxygen, suggesting that all the compounds, upon intersystem crossing (ISC), can produce singlet oxygen ($^1O_2$).

The fluorescence spectra of BTs display a large stokes shift, especially in PBS/DMSO. The fluorescence decay is multi-exponential with average lifetimes below 1 ns for all oligothiophenes (Table S3‡). Likely, the dye can exist in multiple conformations/aggregation states displaying different lifetimes. The study was completed by measuring the emission spectra and fluorescence lifetime of the BT-loaded beads on a confocal microscope as well as the lifetime. Except for **BTO-T2**, the confocal spectra in Fig. S6‡ depend on the selected area in the sample, indicating that the oligothiophenes are likely experiencing different local environments. This lack of homogeneity is

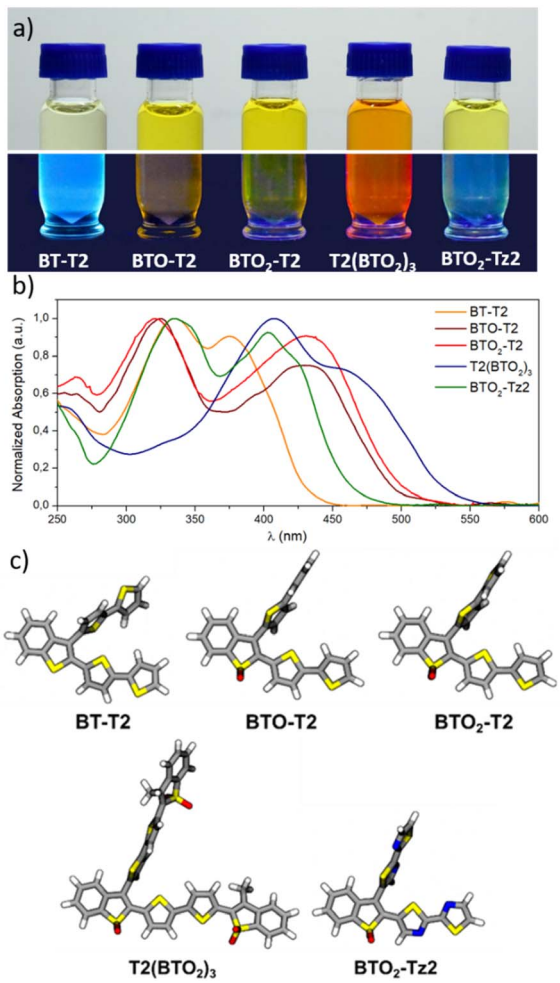

Fig. 3 (a) images of BT solution in CH_2Cl_2 under white light (top) and UV light (λ = 365 nm, bottom), (b) absorption spectra in CH_2Cl_2 and (c) DFT optimized geometries, for **BT-T2**, **BTO-T2**, **BTO_2-T2**, **T2(BTO_2)$_3$** and **BTO_2-Tz2**.

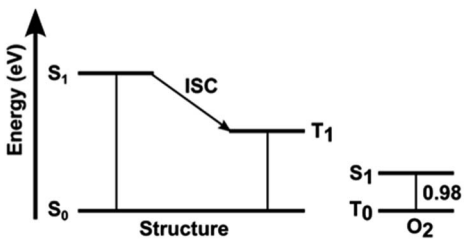

Fig. 4 Jablonski diagrams for BT molecules.

Table 1 Values of the calculated singlet and triplet energies related to the studied BT molecules

Structure	S_1 (eV)	T_1 (eV)
BT-T2	3.45	2.07
BTO-T2	3.06	1.57
BTO_2-T2	3.06	1.51
T2(BTO_2)$_3$	2.95	1.50
BTO_2-Tz2	3.21	1.68

also confirmed by the FLIM images where we can discriminate areas with different average fluorescence lifetimes (Fig. S2b‡).

Reactive oxygen species (ROS) generation by BT molecules and Alg–BT aerogels

The ability of the different BT molecules and related alginate aerogels to produce ROS, upon irradiation, was determined by spectrophotometric measurements, as shown in Fig. 5 (experimental details in ESI, Section 3‡).

Both the mechanisms of ROS production were investigated, by using (i) the Amplex Red assay to quantify the generation of peroxides (type I mechanism)[71–74] and (ii) the 9,10-anthracenediyl-bis(methylene)dimalonic acid (ABMDMA) assay to quantify the production of singlet oxygen (type II mechanism).[75–78] The results summarized in Fig. 5a and b show that all the synthesized BT molecules are suitable photosensitizers, capable of producing ROS following both mechanisms. The different efficiencies in ROS generation, upon irradiation, can be ascribed to the different absorption coefficients of the molecules at the wavelength used for irradiation, *i.e.*, 460 nm, with **T2(BTO$_2$)$_3$** characterized by the highest absorption coefficient and larger oscillator strength.

Interestingly, the photosensitizing behaviour of Alg–BT aerogels changes substantially with respect to the molecules in solution (Fig. 5c). The possibility of generating ROS *via* the type II pathway seems hampered; indeed when the molecules are dispersed in the alginate matrix, the production of singlet oxygen is not detected. Differently, the ability of the Alg–BT aerogels to produce ROS *via* the type I pathway is preserved for all the alginate embedded molecules (Fig. 5c) and the trend observed in solution is almost maintained, with a better performance of **BTO$_2$-Tz2** compared to solution.

This effect is not due to the reaction of $^1O_2$ with the alginate matrix, because when the experiment is repeated with thiophenes in solution, in the presence of empty alginate beads or alginate in solution, the production of singlet oxygen is unaffected. The dispersion of the BTs in the alginate matrix affects their photophysical properties. Oligothiophene molecules exhibit different fluorescence spectra according to the selected area on the beads, indicating that their photophysical behaviour is influenced by the alginate matrix. In addition, confocal imaging shows that the thiophene dyes tend to accumulate in the pores of the alginate beads.

Aggregation is known to drastically reduce the singlet oxygen production efficiency[79] primarily due to triplet–triplet annihilation. However, the persistence of the type I mechanism could be attributed to the specific chemical environment. Electron-rich environments may facilitate the photoactivation switch from type II to type I mechanisms. This effect can be observed when photosensitizers are dispersed in micelles[80] or conjugated to proteins.[81] A sacrificial electron donor is generally required to activate the type I mechanism.[82] The environment inside the beads is extremely electron rich, due to the presence of the carboxylate groups in the alginate matrix. We investigated computationally the possibility to form an anion radical, in the case of **BTO$_2$-Tz2** (Fig. S7‡). The excited state of **BTO$_2$-Tz2** can receive an electron from the carboxylates, forming the anion radical (Fig. S8‡), while the alginate undergoes decarboxylation. The production of a CO_2 molecule is the driving force (entropy-

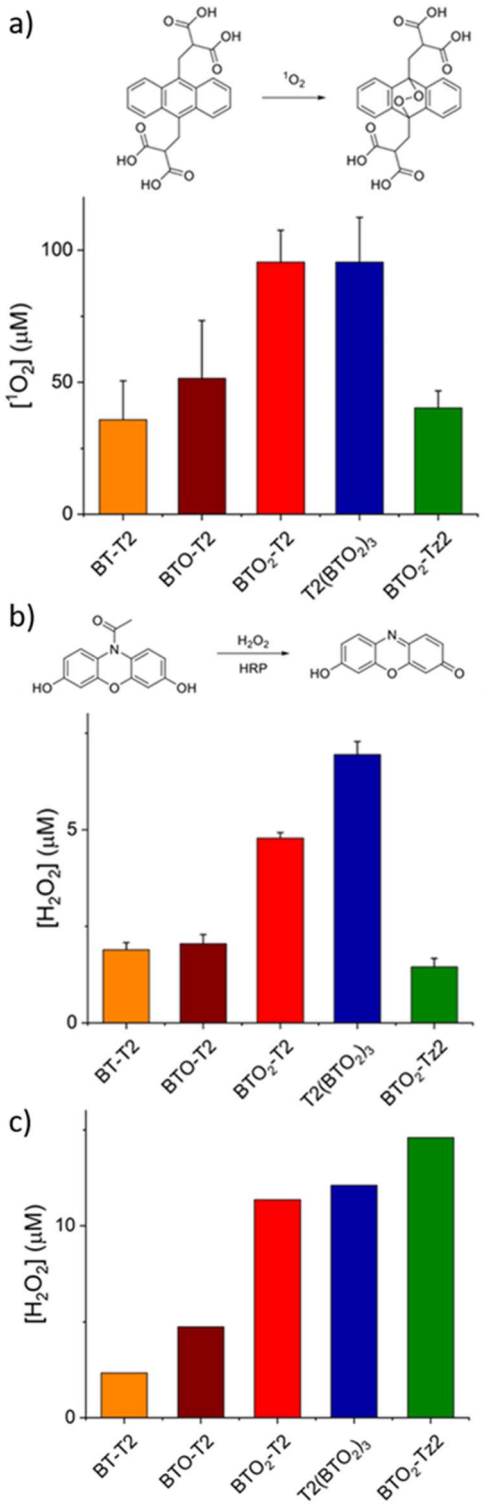

Fig. 5 Generation of ROS after 1 hour of irradiation with a blue LED (10 mW cm^{-2}). (a) Quantification of $^1O_2$ production (type II mechanism) using the ABMDMA colorimetric assay by BT molecules. Quantification of the production of hydrogen peroxide (type I mechanism) *via* the Amplex Red fluorometric assay (b) by BT molecules and (c) by Alg–BT aerogels.

driven reaction) of the process and makes it exothermic. In this case, the formation of ROS *via* the type I mechanism, is due to an electron transfer process involving the ground state of the oxygen molecule rather than the short-lived $^1O_2$. In fact, negatively charged radicals can react with oxygen, eventually leading to H_2O_2 formation in an aqueous environment.[83]

Photodegradation experiments

All Alg–BT aerogels were tested for the photodegradation of the three different ECs, *i.e.* RhB, BPA and OFLOX (Fig. 6a), under blue visible light with $\lambda_{max} = 460$ nm, and the experimental set-up is shown in Fig. 6b–d. A solution of the given contaminant was gently stirred in the presence of Alg–BT aerogels for a total of 5 h and samples were collected every hour to perform HPLC analysis detecting the concentration of the ECs and allowing for the calculation of the degradation percentage (details in ESI, Section 5‡). In detail, the degradation percentage was calculated as a ratio between the detected contaminant concentration after the photodegradation cycle and the initial spiked solution concentration. Control samples of each contaminant without photocatalysts were treated under the same conditions to evaluate the potential effect of interaction between radiation and the water-soluble contaminant molecule. The possible adsorption of the three contaminants by alginate beads has been excluded in previously reported experiments.[70] Fig. 7 shows the EC degradation percentage as a function of irradiation time. RhB, BPA and OFLOX showed negligible degradation without photocatalysts, proving the photostability of these ECs under the experimental conditions used.

The results obtained from the five photocatalysts (Alg–**BT-T2**, Alg–**BTO-T2**, Alg–**BTO_2-T2**, Alg–**T2(BTO_2)$_3$**, and Alg–**BTO_2-Tz2**) showed a common trend for all the tested ECs. Alg–**BTO_2-Tz2** reached a photodegradation percentage higher than 99% within 2 h of contact time for RhB and OFLOX and 3 h for BPA,

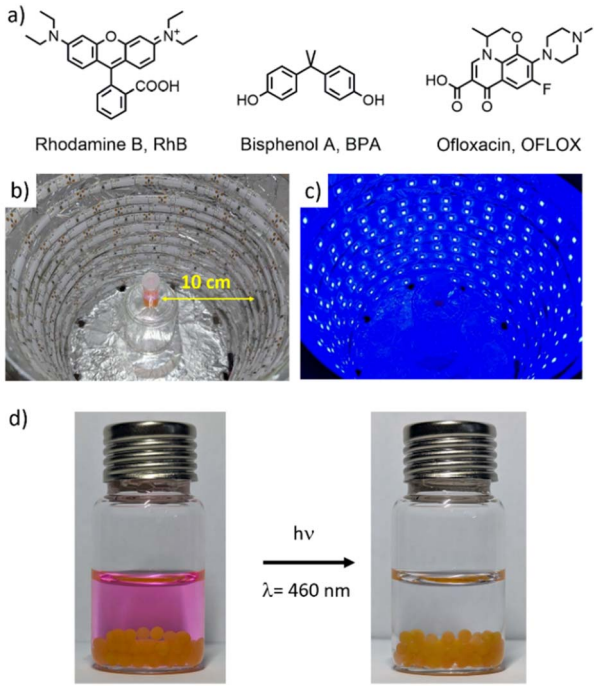

Fig. 6 (a) Chemical structure of the selected emerging contaminants (ECs), (b) photoreactor used in degradation experiments with LED off and (c) LED on. (d) Alg–BT aerogels (Alg–**BTO_2-T2** in the image) were suspended in contaminant spiked water (RhB case study in the image) and irradiated with blue visible light at room temperature.

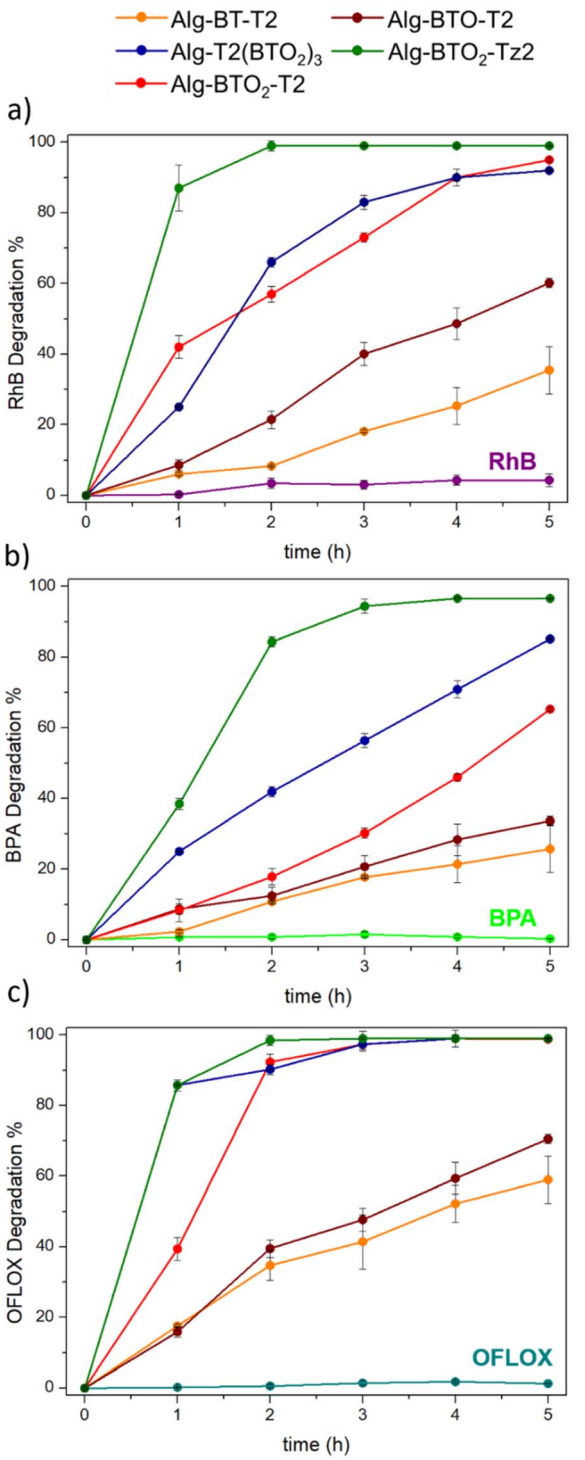

Fig. 7 % Degradation of (a) RhB, (b) BPA, and (c) OFLOX obtained by Alg–BT aerogels ($V = 3$ mL, $C_{IN} = 4$ mg L^{-1}, 5 mg of photocatalysts).

making it the fastest photocatalyst among those tested. Alg–**BTO$_2$-T2** and Alg–**T2(BTO$_2$)$_3$** showed comparable performance towards RhB and OFLOX, achieving complete degradation in 4 h and 3 h of contact time, respectively. For BPA, Alg–**T2(BTO$_2$)$_3$** showed higher degradation capacity, reaching 85% in 5 h, compared to Alg–**BTO$_2$-T2** which showed a slightly lower degradation percentage (65%). The best performances in the degradation of the three ECs tested, were achieved by using Alg–**BTO$_2$-Tz2** and Alg–**BTO$_2$-T2** with the trend that closely matches the amount of ROS generated by the Alg–BT aerogels, reported in Fig. 5c. The ability to reuse photocatalytic materials is fundamental for reducing waste generation and process costs. With the aim of assessing the potential of recycling the photocatalysts for multiple reuses, the stability of the best performing Alg–BTs aerogels (Alg–**BTO$_2$-T2**, Alg–**T2(BTO$_2$)$_3$**, and Alg–**BTO$_2$-Tz2**) was investigated (Fig. 8a).

Photodegradation of RhB, BPA and OFLOX was performed for five consecutive runs. At the end of each cycle, the floating aerogels were quickly recovered from the solution by using a small colander and reused for the next run after washing with deionized water.

Interestingly, after five consecutive runs, no significant change was observed in the degradation efficiency of RhB for any of the BT photocatalysts, with degradation percentages ranging from 89% to 96%. A similar trend was observed for the other pollutants studied: specifically, OFLOX was completely degraded (98–99%), and BPA degradation ranged from 59% to 65% for Alg–**BTO$_2$-T2**, from 79% to 85% for Alg–**T2(BTO$_2$)$_3$**, and from 93% to 96% for Alg–**BTO$_2$-Tz2** (Fig. S9, ESI‡).

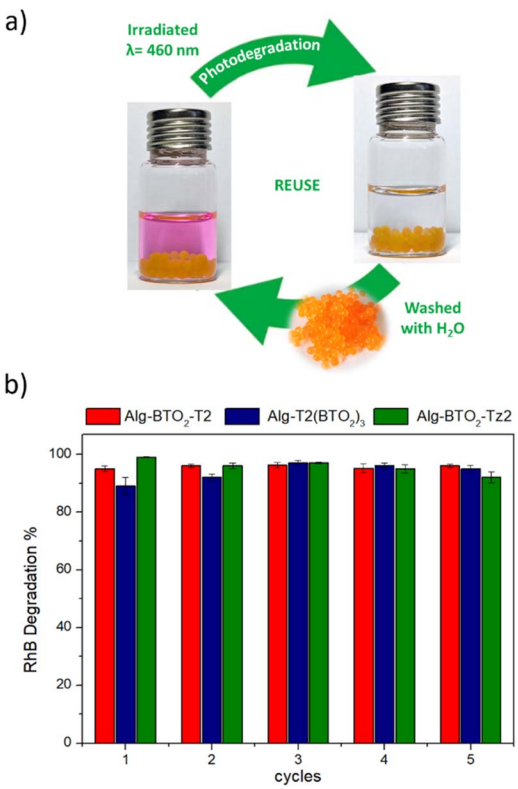

Fig. 8 (a) Sketch of the photodegradation (irradiated at $\lambda = 460$ nm) and reuse process (aerogels washed with deionized water). (b) Recycling of Alg–**BTO$_2$-T2**, Alg–**T2(BTO$_2$)$_3$** and Alg–**BTO$_2$-Tz2** aerogels on RhB showed as a case study (BPA/OFLOX, in Fig. S9, ESI‡).

Ecotoxicity experiments

Water solutions of OFLOX were analysed with the bioluminescent bacterium *A. fischeri* to assess the possible intrinsic acute ecotoxicity and, in the case of irradiated solutions, the ecotoxicity of degradation by-products. The bioluminescent bacterium *A. fischeri*, was exposed for 5, 15 and 30 minutes to solutions in accordance with the standardised method and the experimental details are reported in Section 6, ESI.‡[62]

The effects are considered toxic if the inhibition of bioluminescence is >20% (toxicity threshold) compared to the light emission of the bacterium under optimal conditions (in saline solution, 20 g per L NaCl).[84] The effects are reported as average values % of bioluminescence inhibition (±standard error). The 30-min toxicity results are shown in Fig. 9; results for all exposure times (5, 15 and 30 min) are reported in Table S4 in ESI.‡ All solutions showed no toxic effects at any of the exposure times on *A. fischeri*. Indeed, bioassays on the OFLOX antibiotic and its irradiated solutions showed values below the ecotoxicity threshold (<20%), with bioluminescence inhibition values ranging between 0% and 11.64%.

Consequently, the irradiated antibiotic with and without the photocatalyst displayed no ecotoxicity. In particular, OFLOX in water displays a bioluminescence inhibition of 6.91% ± 1.23%, and the antibiotic irradiated in the presence of the photocatalyst (OFLOX + Alg–**BTO$_2$-T2** + UV) displayed even lower inhibition (0.93% ± 0.42%). This means that the photodegradative by-products were not toxic, showing even lower inhibition compared to the starting OFLOX solution. In addition to OFLOX solutions, the test was also performed on ultrapure water left in contact with the Alg–**BTO$_2$-T2** aerogel in the absence of light. In this case, the solution proved to be non-toxic and no bioluminescence inhibition was observed. This confirms that the BT molecules are stable and are not released into water, once encapsulated in the alginate matrices. Finally, Alg–**BTO$_2$-T2** aerogels in water were irradiated in the absence of OFLOX as a control, and the resulting solution (Alg–**BTO$_2$-T2** + UV) was analysed under the same conditions. The solution was

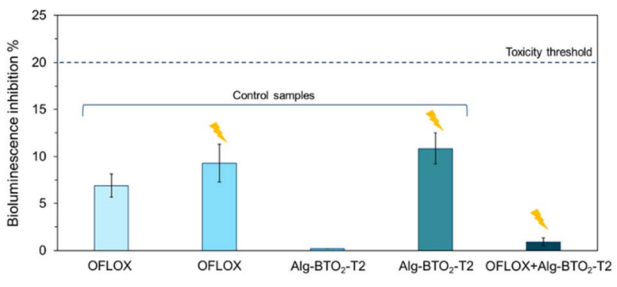

Fig. 9 *A. fischeri* bioluminescence inhibition% at 30 min induced by solutions containing (from left to right): OFLOX kept in the absence of light, OFLOX irradiated, Alg–BTO_2 in the absence of light, Alg–BTO_2 irradiated, and OFLOX irradiated in the presence of Alg–**BTO$_2$-T2** aerogels. The flash highlights the irradiated samples.

not toxic being below the 20% threshold but displayed the highest bioluminescence inhibition (10.86% ± 1.65%) compared to the other samples. Probably, in the absence of contaminants to be degraded, the radicals formed during irradiation cause oxidative stress to *A. fischeri*.

Conclusions

A family of V-shaped oligothiophenes, derived from a benzo[*b*]thiophene (BT) core and *S*-oxide or *S*,*S*-dioxide moieties, was synthesized by the Stille cross-coupling reaction, with yields in the range of 67–83%. The optical properties of BT molecules were studied by spectroscopy and DFT calculations. Upon blue-light irradiation, the targeted BT molecules demonstrated the ability to generate ROS following both type I and type II mechanisms. BT molecules were encapsulated in an alginate matrix by ionotropic gelation–freeze drying, resulting in porous aerogels that were dispersed in water and tested in the photodegradation of three emerging contaminants, *i.e.*, RhB, BPA and OFLOX. Among the synthesized alginate–BT aerogels, Alg–**BTO_2-Tz2** proved to be the best performing photocatalyst, achieving complete degradation of all the three ECs within 2 h, followed by Alg–**BTO_2-T2** and Alg–**T2(BTO_2)$_3$**, which still showed high efficiency (complete degradation in less than 5 h). This trend perfectly reproduces the amount of ROS generated by the Alg–BT aerogels and the obtained results highlight the important role of the *S*,*S*-dioxide moiety in the generation of ROS. The stability of the aerogels was evaluated by performing five photodegradation cycles with the same photocatalysts, showing no noticeable change in degradation efficiency, proving the reusability of the photocatalysts. Furthermore, an ecotoxicological bioassay using *Aliivibrio fischeri* was performed on the OFLOX antibiotic and its photodegradation by-products. Both solutions showed no toxicity (values below the threshold: inhibition of bioluminescence < 20%), and the photodegradation by-products displayed less bioluminescence inhibition in the bacterium, lower than the initial OFLOX solution. This work demonstrates the possibility of exploiting oligothiophenes as photocatalysts and sheds some light on the structure–properties relationships in *S*-oxide and *S*,*S*-dioxide based materials, opening new perspectives for water treatment and the degradation of persistent emerging contaminants.

Data availability

Detailed description of materials synthesis and characterization, theoretical calculations, light-induced reactive oxygen species quantification, photodegradation experiments, high performance liquid chromatography analyses, and ecotoxicity experiments.

Author contributions

Andrea Trifoglio: methodology, investigation, data curation, editing. Francesca Tunioli: methodology, investigation, data curation, editing. Laura Favaretto: methodology, investigation. Massimo Zambianchi: methodology, investigation. Cristian Bettini: methodology, investigation. Ilse Manet: methodology, investigation, formal analysis. Livia Mariani: methodology, investigation. Anna Barra Caracciolo: methodology, investigation. Paola Grenni: methodology, investigation. Manuele Di Sante: investigation, methodology, formal analysis. Matteo Di Giosia: investigation, methodology, formal analysis. Tainah Dorina Marforio: investigation, methodology, formal analysis. Edoardo Jun Mattioli: investigation, methodology, formal analysis. Matteo Calvaresi: investigation conceptualization. Manuela Melucci: conceptualization, validation, writing – original draft.

Conflicts of interest

There are no conflicts of interest to declare.

Acknowledgements

The authors gratefully acknowledge the support for this work by the projects Life-Remembrance, ENV/IT/001001 Life Resource and Environment LIFE20 'Give plastic wastes from the production of hollow-fiber membranes a second life', project PNRR MUR project ECS_00000033_ECOSISTER, and 'Le materie prime del futuro da fonti non-critiche, residuali e rinnovabili' (FUTURAW, FOE 2022). Edoardo Jun Mattioli was supported by Fondazione Umberto Veronesi.

Notes and references

1 F. Xiao, B. Deng, D. Dionysiou, T. Karanfil, K. O'Shea, P. Roccaro, Z. J. Xiong and D. Zhao, *Nat. Water*, 2023, **1**, 1004–1015.
2 B. Rathi, P. Kumar and D.-V. Vo, *Sci. Total Environ.*, 2021, **797**, 149134.
3 X. Tong, S. Mohapatra, J. Zhang, N. H. Tran, L. You, Y. He and K. Y.-H. Gin, *Water Res.*, 2022, **217**, 118418.
4 O. S. Arvaniti and A. S. Stasinakis, *Sci. Total Environ.*, 2015, **524–525**, 81–92.
5 **https://www.epa.gov/sdwa/and-polyfluoroalkyl-substances-pfas**.
6 P. Thamarai, R. Kamalesh, A. Saravanan, P. Swaminaathan and V. C. Deivayanai, *Environ. Nanotechnol., Monit. Manage.*, 2024, **21**, 100913.
7 H. Azzahra, A. F. Nisaa and M. A. Mardyanto, *IOP Conf. Ser. Earth Environ. Sci.*, 2024, **1307**, 012013.
8 D. Yadav, S. Karki and P. G. Ingole, *J. Environ. Chem. Eng.*, 2022, **10**, 108109.
9 M. M. Zubair, H. Saleem and S. J. Zaidi, *Desalination*, 2023, **564**, 116705.
10 S. Feijoo, X. Yu, M. Kamali, L. Appels and R. Dewil, *Rev. Environ. Sci. Bio/Technol.*, 2023, **22**, 205–248.
11 J. Yuan, E. Passeport and R. Hofmann, *Water Res.*, 2022, **210**, 118026.
12 E. Menya, J. Jjagwe, H. M. Kalibbala, H. Storz and P. W. Olupot, *Chem. Eng. Res. Des.*, 2023, **192**, 412–440.
13 A. Katsigiannis, C. Noutsopoulos, J. Mantziaras and M. Gioldasi, *Chem. Eng. J.*, 2015, **280**, 49–57.

14 N. Singh, G. Nagpal and S. Agrawal, *Environ. Technol. Innovation*, 2018, **11**, 187–240.
15 M. N. Soliman, F. Z. Guen, S. A. Ahmed, H. Saleem, M. J. Khalil and S. J. Zaidi, *Process Saf. Environ. Prot.*, 2021, **147**, 589–608.
16 D. Van Thuan, H. L. Ngo, H. P. Thi and T. T. H. Chu, *Environ. Res.*, 2023, **229**, 116000.
17 H. C. Yap, Y. L. Pang, S. Lim, A. Z. Abdullah, H. C. Ong and C. H. Wu, *Int. J. Environ. Sci. Technol.*, 2019, **16**, 601–628.
18 H. Kumari, S. Sonia, R. Ranga, S. Chahal, S. Devi, S. Sharma, S. Kumar, P. Kumar, S. Kumar, A. Kumar and R. Parmar, *Water, Air, Soil Pollut.*, 2023, **234**, 349.
19 S. Peiris, H. B. de Silva, K. N. Ranasinghe, S. V. Bandara and I. R. Perera, *J. Chin. Chem. Soc.*, 2021, **68**, 738–769.
20 S. Murgolo, S. Franz, H. Arab, M. Bestetti, E. Falletta and G. Mascolo, *Water Res.*, 2019, **164**, 114920.
21 M. N. Chong, B. Jin, C. W. K. Chow and C. Saint, *Water Res.*, 2010, **44**, 2997–3027.
22 S.-Y. Lee and S.-J. Park, *J. Ind. Eng. Chem.*, 2013, **19**, 1761–1769.
23 V. Prashanth, P. Jayasree, P. Rajput and N. Remya, in *Advanced Oxidation Processes for Effluent Treatment Plants*, ed. M. P. Shah, Elsevier, 2021, pp. 69–85, DOI: 10.1016/B978-0-12-821011-6.00004-9.
24 S. Ramu, I. Kainthla, L. Chandrappa, J. M. Shivanna, B. Kumaran and R. G. Balakrishna, *Environ. Sci. Pollut. Res. Int.*, 2024, **31**, 167–190.
25 X. Li, K. Kawai, M. Fujitsuka and Y. Osakada, *Surf. Interfaces*, 2021, **25**, 101249.
26 Y. Feng, X. Su, Y. Chen, Y. Liu, X. Zhao, C. Lu, Y. Ma, G. Lu and M. Ma, *Mater. Res. Bull.*, 2023, **162**, 112207.
27 C. Santhosh, V. Velmurugan, G. Jacob, S. K. Jeong, A. N. Grace and A. Bhatnagar, *Chem. Eng. J.*, 2016, **306**, 1116–1137.
28 A. Feliczak-Guzik, *Materials*, 2023, **16**, 193.
29 Q. Wang, Q. Gao, A. M. Al-Enizi, A. Nafady and S. Ma, *Inorg. Chem. Front.*, 2020, **7**, 300–339.
30 L. Gan, M. T. Nord, J. M. Lessard, N. Q. Tufts, A. Chidambaram, M. E. Light, H. Huang, E. Solano, J. Fraile, F. Suárez-García, C. Viñas, F. Teixidor, K. C. Stylianou and J. G. Planas, *J. Am. Chem. Soc.*, 2023, **145**, 13730–13741.
31 H. Jia, D. Ma, S. Zhong, L. Li, L. Li, L. Xu and B. Li, *Chem. Eng. J.*, 2019, **368**, 165–174.
32 S. Silvestri, A. R. Fajardo and B. A. Iglesias, *Environ. Chem. Lett.*, 2022, **20**, 731–771.
33 K. S. Min, R. Manivannan and Y.-A. Son, *Dyes Pigm.*, 2019, **162**, 8–17.
34 M. Moosavifar, S. M. Heidari, L. Fathyunes, M. Ranjbar, Y. Wang and H. Arandiyan, *J. Inorg. Organomet. Polym. Mater.*, 2020, **30**, 1621–1628.
35 H. Ozawa, S. Kusaba, M. Matsunaga and M.-a. Haga, *Langmuir*, 2018, **34**, 2952–2958.
36 L.-S. Wan, J. Wu and Z.-K. Xu, *Macromol. Rapid Commun.*, 2006, **27**, 1533–1538.
37 Z.-L. Ma, G.-F. Huang, D.-S. Xu, M.-G. Xia, W.-Q. Huang and Y. Tian, *Mater. Lett.*, 2013, **108**, 37–40.
38 D. M. Mafukidze and T. Nyokong, *J. Photochem. Photobiol., A*, 2021, **409**, 113142.
39 W.-j. Sun, J. Li, G.-p. Yao, F.-x. Zhang and J.-L. Wang, *Appl. Surf. Sci.*, 2011, **258**, 940–945.
40 R. Rahimi, S. Zargari, A. Ghaffarinejad and A. Morsali, *Environ. Prog. Sustainable Energy*, 2016, **35**, 642–652.
41 A. Gogoi, P. Mazumder, V. K. Tyagi, G. G. Tushara Chaminda, A. K. An and M. Kumar, *Groundw. Sustain. Dev.*, 2018, **6**, 169–180.
42 A. Tkaczyk, K. Mitrowska and A. Posyniak, *Sci. Total Environ.*, 2020, **717**, 137222.
43 T. L. Yusuf, B. O. Orimolade, D. Masekela, B. Mamba and N. Mabuba, *RSC Adv.*, 2022, **12**, 26176–26191.
44 J. Sharma, S. Sharma, U. Bhatt and V. Soni, *J. Hazard. Mater. Lett.*, 2022, **3**, 100069.
45 Y. Qian, X. Jia, T. Ding, M. Yang, B. Yang and J. Li, *Sci. Total Environ.*, 2021, **758**, 143606.
46 L. E. Lesser, A. Mora, C. Moreau, J. Mahlknecht, A. Hernández-Antonio, A. I. Ramírez and H. Barrios-Piña, *Chemosphere*, 2018, **198**, 510–521.
47 P. Kovalakova, L. Cizmas, T. J. McDonald, B. Marsalek, M. Feng and V. K. Sharma, *Chemosphere*, 2020, **251**, 126351.
48 G. Barbarella, L. Favaretto, A. Zanelli, G. Gigli, M. Mazzeo, M. Anni and A. Bongini, *Adv. Funct. Mater.*, 2005, **15**, 664–670.
49 G. Barbarella, L. Favaretto, G. Sotgiu, M. Zambianchi, V. Fattori, M. Cocchi, F. Cacialli, G. Gigli and R. Cingolani, *Adv. Mater.*, 1999, **11**, 1375–1379.
50 C. Santato, L. Favaretto, M. Melucci, A. Zanelli, M. Gazzano, M. Monari, D. Isik, D. Banville, S. Bertolazzi, S. Loranger and F. Cicoira, *J. Mater. Chem.*, 2010, **20**, 669–676.
51 R. Peng, Y. Luo, Q. Cui, J. Wang and L. Li, *ACS Appl. Bio Mater.*, 2020, **3**, 1305–1311.
52 A. Cantelli, M. Malferrari, A. Soldà, G. Simonetti, S. Forni, E. Toscanella, E. J. Mattioli, F. Zerbetto, A. Zanelli, M. Di Giosia, M. Zangoli, G. Barbarella, S. Rapino, F. Di Maria and M. Calvaresi, *JACS Au*, 2021, **1**, 925–935.
53 M. Piacenza, M. Zambianchi, G. Barbarella, G. Gigli and F. Della Sala, *Phys. Chem. Chem. Phys.*, 2008, **10**, 5363–5373.
54 R. A. Raus, W. M. F. W. Nawawi and R. R. Nasaruddin, *Asian J. Pharm. Sci.*, 2021, **16**, 280–306.
55 Y. Sun, T. Zhou, W. Li, F. Yu and J. Ma, *Chemosphere*, 2020, **241**, 125110.
56 D. Eluk, O. Nagel, A. Gagneten, U. Reno and R. Althaus, *Water Environ. Res.*, 2021, **93**, 2914–2930.
57 T.-D. Nguyen, T. Itayama, R. Ramaraj, N. Iwami, K. Shimizu, T.-S. Dao, T.-L. Pham and H. Maseda, *Environ. Pollut.*, 2021, **291**, 118095.
58 T.-D. Nguyen, T. Itayama, N. Iwami, K. Shimizu, T.-S. Dao, T. L. Pham, V. Q. Tran and H. Maseda, *Drug Chem. Toxicol.*, 2023, **47**(5), 662–673.
59 S. Jouanneau, M.-J. Durand-Thouand and G. Thouand, *Environ. Sci. Pollut. Res.*, 2016, **23**, 4340–4345.
60 S. Parvez, C. Venkataraman and S. Mukherji, *Environ. Int.*, 2006, **32**, 265–268.

61 M. Abbas, M. Adil, S. Ehtisham-ul-Haque, B. Munir, M. Yameen, A. Ghaffar, G. A. Shar, M. Asif Tahir and M. Iqbal, *Sci. Total Environ.*, 2018, **626**, 1295–1309.
62 L. Mariani, P. Grenni, A. Barra Caracciolo, E. Donati, J. Rauseo, L. Rolando and L. Patrolecco, *Ecotoxicology*, 2020, **29**, 815–824.
63 H. Shimotani, S. Ikeda, N. Asao, Y. Yamamoto, K. Tanigakiab and T. Jin, *Chem. Commun.*, 2016, **52**, 4926–4929.
64 J. Hassan, L. Lavenot, C. Gozzi and M. Lemaire, *Tetrahedron Lett.*, 1999, **40**, 857–858.
65 M. J. T. Frisch, G. W. Trucks, H. B. Schlegel, G. E. Scuseria, M. A. Robb, J. R. Cheeseman, G. Scalmani, V. Barone, B. Mennucci, G. A. Petersson, H. Nakatsuji, M. Caricato, X. Li, H. P. Hratchian, A. F. Izmaylov, J. Bloino, G. Zheng, J. L. Sonnenberg, M. Hada, M. Ehara, K. Toyota, R. Fukuda, J. Hasegawa, M. Ishida, T. Nakajima, Y. Honda, O. Kitao, H. Nakai, T. Vreven, J. A. Montgomery Jr, J. E. Peralta, F. Ogliaro, M. J. Bearpark, J. Heyd, E. N. Brothers, K. N. Kudin, V. N. Staroverov, R. Kobayashi, J. Normand, K. Raghavachari, A. P. Rendell, J. C. Burant, S. S. Iyengar, J. Tomasi, M. Cossi, N. Rega, N. J. Millam, M. Klene, J. E. Knox, J. B. Cross, V. Bakken, C. Adamo, J. Jaramillo, R. Gomperts, R. E. Stratmann, O. Yazyev, A. J. Austin, R. Cammi, C. Pomelli, J. W. Ochterski, R. L. Martin, K. Morokuma, V. G. Zakrzewski, G. A. Voth, P. Salvador, J. J. Dannenberg, S. Dapprich, A. D. Daniels, O. Farkas, J. B. Foresman, J. V. Ortiz, J. Cioslowski and D. J. Fox, *Gaussian16*, Wallingford, CT, 2016.
66 M. Cossi, V. Barone, R. Cammi and J. Tomasi, *Chem. Phys. Lett.*, 1996, **255**, 327–335.
67 T. Yanai, D. P. Tew and N. C. Handy, *Chem. Phys. Lett.*, 2004, **393**, 51–57.
68 S. Canola, L. Mardegan, G. Bergamini, M. Villa, A. Acocella, M. Zangoli, L. Ravotto, S. A. Vinogradov, F. Di Maria and P. Ceroni, *Photochem. Photobiol. Sci.*, 2019, **18**, 2180–2190.
69 B. Wang, Y. Wan, Y. Zheng, X. Lee, T. Liu, Z. Yu, J. Huang, Y. S. Ok, J. Chen and B. Gao, *Crit. Rev. Environ. Sci. Technol.*, 2019, **49**, 318–356.
70 F. Tunioli, S. Khaliha, S. Mantovani, A. Bianchi, A. Kovtun, Z. Xia, M. S. S. Bafqi, B. S. Okan, T. D. Marforio, M. Calvaresi, V. Palermo, M. L. Navacchia and M. Melucci, *J. Environ. Chem. Eng.*, 2023, **11**, 109566.
71 E. Turrini, L. Ulfo, P. E. Costantini, R. Saporetti, M. Di Giosia, M. Nigro, A. Petrosino, L. Pappagallo, A. Kaltenbrunner, A. Cantelli, V. Pellicioni, E. Catanzaro, C. Fimognari, M. Calvaresi and A. Danielli, *Cell. Mol. Life Sci.*, 2024, **81**, 144.
72 A. Petrosino, R. Saporetti, F. Starinieri, E. Sarti, L. Ulfo, L. Boselli, A. Cantelli, A. Morini, S. K. Zadran and G. Zuccheri, *iScience*, 2023, **26**, 108032.
73 B. Bortot, M. Apollonio, G. Baj, L. Andolfi, L. Zupin, S. Crovella, M. di Giosia, A. Cantelli, R. Saporetti, L. Ulfo, A. Petrosino, G. Di Lorenzo, F. Romano, G. Ricci, M. Mongiat, A. Danielli, M. Calvaresi and S. Biffi, *Free Radical Biol. Med.*, 2022, **179**, 242–251.
74 L. Ulfo, A. Cantelli, A. Petrosino, P. E. Costantini, M. Nigro, F. Starinieri, E. Turrini, S. K. Zadran, G. Zuccheri and R. Saporetti, *Nanoscale*, 2022, **14**, 632–641.
75 M. Di Sante, A. Kaltenbrunner, M. Lombardo, A. Danielli, P. E. Costantini, M. Di Giosia and M. Calvaresi, *Pharmaceuticals*, 2023, **16**, 1329.
76 A. Marconi, G. Giugliano, M. Di Giosia, T. D. Marforio, M. Trivini, E. Turrini, C. Fimognari, F. Zerbetto, E. J. Mattioli and M. Calvaresi, *Pharmaceutics*, 2023, **15**, 919.
77 G. Greco, L. Ulfo, E. Turrini, A. Marconi, P. E. Costantini, T. D. Marforio, E. J. Mattioli, M. Di Giosia, A. Danielli and C. Fimognari, *Cells*, 2023, **12**, 392.
78 E. J. Mattioli, L. Ulfo, A. Marconi, V. Pellicioni, P. E. Costantini, T. D. Marforio, M. Di Giosia, A. Danielli, C. Fimognari and E. Turrini, *Biomolecules*, 2022, **13**, 68.
79 C. Alvarez-Lopez, D. Cavazos-Elizondo, B. Heyne, I. E. Kochevar and A. Aguirre-Soto, *Photochem. Photobiol.*, 2023, **99**, 580–592.
80 H. Ding, H. Yu, Y. Dong, R. Tian, G. Huang, D. A. Boothman, B. D. Sumer and J. Gao, *J. Controlled Release*, 2011, **156**, 276–280.
81 A. Cantelli, F. Piro, P. Pecchini, M. Di Giosia, A. Danielli and M. Calvaresi, *J. Photochem. Photobiol., B*, 2020, **206**, 111852.
82 P. Sanchez-Cruz, F. Dejesus-Andino and A. E. Alegria, *J. Photochem. Photobiol., A*, 2012, **236**, 54–60.
83 K. Plaetzer, B. Krammer, J. Berlanda, F. Berr and T. Kiesslich, *Lasers Med. Sci.*, 2009, **24**, 259–268.
84 G. Persoone, B. Marsalek, I. Blinova, A. Törökne, D. Zarina, L. Manusadzianas, G. Nalecz-Jawecki, L. Tofan, N. Stepanova, L. Tothova and B. Kolar, *EnTox*, 2003, **18**, 395–402.